Advances in Water Resources 103 (2017) 86–98

Contents lists available at ScienceDirect

Advances in Water Resources

journal homepage: www.elsevier.com/locate/advwatres

Probabilistic predictions using a groundwater model informed with airborne EM data

Pernille Aabye Marker[a,*], Troels Norvin Vilhelmsen[b], Nikolaj Foged[b], Thomas Wernberg[c], Esben Auken[b], Peter Bauer-Gottwein[a]

[a] Department of Environmental Engineering, Technical University of Denmark, Bygningstorvet, building 115, 2800 Kgs. Lyngby, Denmark
[b] HydroGeophysics Group, Department of Geoscience, Aarhus University, C.F. Møllers Allé 4, building 1120, 8000 Aarhus C, Denmark
[c] NIRAS Aarhus, Ceres alle 3, 8000 Aarhus C, Denmark

ARTICLE INFO

Article history:
Received 28 April 2016
Revised 4 March 2017
Accepted 5 March 2017
Available online 6 March 2017

Keywords:
Hydrological prediction uncertainty
Hydrostratigraphic uncertainty
Hydrogeophysical inversion
Airborne electromagnetics
Well catchment area

ABSTRACT

Some hydrological model predictions are particularly sensitive to the hydrostratigraphy of numerical groundwater models, which are used extensively in the management of groundwater resources. In this paper we present a method to estimate hydrological prediction uncertainty originating from uncertainty in subsurface structure. Densely sampled airborne electromagnetic (AEM) data, which captures the main geological features, along with borehole lithological information are used as input to the hydrostratigraphic models. Geophysical resistivity models obtained from spatially constrained 1-D inversion of the AEM data are translated into clay-fraction values with a spatially variable translator function. Hydrostratigraphic units are identified by *k*-means clustering on the 2-D space defined by estimated resistivity values and clay-fraction values. Areas with no data are represented stochastically using sequential indicator simulation (SIS) where the spatial model of each hydrostratigraphic unit is characterized by an indicator variogram. This results in an ensemble of equally likely hydrostratigraphic representations of the subsurface. A hydraulic conductivity value of each hydrostratigraphic unit of each realization is estimated in a groundwater model calibration constrained by observations of hydraulic head and stream base flow. Pumping well catchment areas are calculated for each realization. The result is a probabilistic well catchment area, which is checked for bias with a manually constructed geological model. There is a probability of 85% of the catchment extending beyond the manually constructed geology. The method is applied to the 45 km^2 large groundwater model of the Kasted site in Denmark. The method presented in the paper has the advantage of being data-driven, making the modeling process entirely reproducible.

1. Introduction

Hydrological models are often developed as decision support tools for the management of surface or groundwater resources. The models are typically set up with a deterministic hydrostratigraphy using available borehole information, geophysical data sets, and expert knowledge. Model parameters (e.g. hydraulic conductivity, K), are subsequently estimated using inversion/calibration. The hydrological observations for this inversion are often limited to head and flow data. Due to the inherent uncertainty of the deterministic representation of the subsurface, these data are insufficient to address prediction uncertainty. Especially flow and transport predictions are often sensitive to hydrostratigraphical variation, while the observations used to inform the hydrological inversion may not be sufficiently sensitive to hydrostratigraphical variation (Rojas et al., 2010; Refsgaard et al., 2012; Seifert et al., 2012). Correspondingly, decision making under risk (based on uncertain hydrological prediction estimates) is receiving attention (Tartakovsky, 2013). Due to the inherent difficulty to map subsurface structures, all hydrostratigraphical models are to some extent flawed. Deterministic approaches are therefore inadequate to address the uncertainty of predictions of flow and transport. Making multiple realizations of model hydrostratigraphy based on manual data interpretation is a tedious and difficult task. Applying automated model building routines based on geostatistical methods provides the means for estimating the structural uncertainty, but has extensive input data requirements. In order to capture variations in the subsurface that can be relevant for groundwater flow, a high spatial data-sampling rate is often necessary. Lithological data from boreholes often have a high vertical resolution, whereas horizontal variability of geological units is often not captured due to the limited borehole density. Airborne Transient Electromagnetic Methods (AEM)

* Corresponding author.
E-mail address: paam@env.dtu.dk (P.A. Marker).

http://dx.doi.org/10.1016/j.advwatres.2017.03.002

is a geophysical method that maps variations in subsurface resistivity. Data are obtained by measuring the decay of a secondary magnetic field, which is caused by the diffusion of electrical currents through subsurface materials induced by a primary transmitter field (Kirsch, 2009). Resistivity models of the subsurface, i.e. the change of resistivity of subsurface materials with depth, are obtained by inverting the data. AEM provides dense horizontal data coverage, but the resistivity models obtained through inversion need to be related to the local lithology, to provide input to hydrological models. Thus, using the combined information held in borehole logs and AEM data in a geostatistical framework makes it possible to estimate the uncertainty related to subsurface structures in hydrological models.

Geostatistical prediction and simulation methods were introduced in inverse hydrological problems decades ago to assist hydrologists to estimate the K field and the associated uncertainty by conditioning to measurements of K and hydraulic head (Delhomme, 1979; Neuman and Yakowitz, 1979). Geostatistical methods provide the opportunity to assess hydrological model parameters and predictions originating from uncertain subsurface structural models probabilistically. Many studies have used two-point geostatistical methods to simulate aquifer structures, see for example Dell' Arciprete et al. (2011); examples of applications in hydrology include Gómez-Hernández (1994) and Klise et al. Klise et al. (2009). The uncertainty in the simulated aquifer structures associated with the choice of simulation algorithm is not addressed in this paper. For such analysis, the reader is referred to for example Dell' Arciprete et al. (2011), who compare SISIM, TProGS and MPS using a 2-D training image. This study focuses on the hydrologic uncertainty represented by the ensemble of subsurface realizations. Multiple-point statistical (MPS) methods are popular because the use of training images makes it possible to represent subsurface structures that are closer to geologic reality Linde et al. (2015), see for example Dickson et al. (2015), Hermans et al. (2015), and Ronayne et al. (2008) for applications in hydrology. Dickson et al. (2015) compared an MPS interpretation to a deterministic interpretation of airborne magnetic data to model the aquifer of a groundwater model. They found that the structural information in the training image improved the fit to hydrological data. Since AEM surveys can cover large areas with high sampling density, the main geological features of a given site can often be captured, which makes the use of a training images less crucial.

Geophysical data are used widely in hydrology, see for example Rubin and Hubbard (2005) and references therein. Geophysical data offer imaging and coverage opportunities of structures relevant for groundwater flow that hydrological data alone cannot constrain. AEM data are unique in terms of coverage and depth of investigation while obtaining a fine enough resolution of the subsurface that is necessary for large-scale groundwater model applications. The data can cover up to hundreds of square kilometers down to depths of 300 m below ground surface. Applications of AEM in hydrogeology include: modeling of 3-D geological structures of unconsolidated sedimentary environments (Burschil et al., 2012; Bosch et al., 2009; Jørgensen et al., 2010; Gunnink and Siemon, 2015; Steinmetz et al., 2014); mapping of saltwater intrusion and anomalies (Sulzbacher et al., 2012; Rasmussen et al., 2013; Chongo et al., 2015); and descriptions of complex hydrological systems (Friedel et al., 2012; Gondwe et al., 2010; Meier et al., 2014).

The use of AEM data in hydrogeophysical inversions (see (Hinnell et al., 2010) for definitions) are rare. Gunnink and Siemon (2015) and He et al. (2015) used variogram models and transition probabilities in a sequential indicator simulation (SIS) framework to probabilistically model the spatial distribution of sand and clay facies. He et al. (2015) applied the method to a subdomain of a hydrological model, and extracted sand and clay information from AEM data using a threshold value determined from comparison of AEM data and lithological borehole logs. K values of the sand and clay facies were determined subsequently through inversion of an integrated hydrological model. A uniform correlation between resistivity and sand/clay across the large domain may be incorrect due to influence of for example variable pore-water conductivity and variable AEM data resolution with depth.

To our knowledge this paper is the first to present a method to estimate structure-dependent probabilistic groundwater model predictions (of states not used for calibration) using hydrogeophysical inversion informed by an AEM data set over a large domain. One of the objectives of this analysis is to address the uncertainty of data scarce areas in the modeled domain is addressed. The method makes use of all primary hydrological, lithological and geophysical data available. The prediction uncertainty is addressed with an ensemble of subsurface model realizations that are automatically generated from borehole information and AEM data. Translation between geophysical and hydrological properties is handled through inversion for a spatially variable relationship between resistivity and lithological observations of clay and *k*-means cluster analysis (Foged et al., 2014; Marker et al., 2015). The number of facies (clusters) to represent the subsurface structures is determined using the hydrological data and model. Utilizing sequential indicator simulation (SIS) the categories are simulated onto a regular grid; forming an ensemble of subsurface structure realizations. Hydraulic properties of each structural realization are estimated with a groundwater model by calibrating the model to head and flow observations. The prediction uncertainty of the model is estimated from the variation in the predicted well catchment area within the ensemble.

The workflow has been applied to a Danish site characterized by glacially formed aquifer systems. This type of Quaternary aquifer systems are of great interest for drinking water supply in Northern European countries like the Netherlands, Northern Germany, and Denmark as well as in the northern part of North America.

2. Materials and methods

A complete overview of the method presented in this paper is shown in Fig. 1. The methods build on previous work by Christiansen et al. (2014), Foged et al. (2014), and Marker et al. (2015). Parts of the workflow applied in this paper have been described in Foged et al. (2014) and Marker et al. (2015), although a different case study was used in these two papers. Foged et al. (2014) present the 3-dimensional clay-fraction procedure along with the combined clustering of clay-fraction and resistivity values. Throughout the paper the estimated parameter values of the resistivity models, which have been obtained through spatially constrained 1-D inversion of the geophysical data, will be referred to as resistivity values. Marker et al. (2015) use the cluster model deterministically (grey boxes in Fig. 1) to represent groundwater model hydrostratigraphy and directly estimate K values of the clusters through hydrological calibration. In this paper the method is extended to create an ensemble of hydrostratigraphic cluster models, and the thick dashed box in Fig. 1 indicates the novelty and the focus of this paper. We use the term 'hydrostratigraphy' to characterize a subsurface model, which is obtained by geostatistical simulation of categorical cluster values. The units that make up the hydrostratigraphy are typically referred to as 'hydrofacies' . However, we use 'hydrostratigraphy' to make it clear that the entire 3-D subsurface model is used directly in a groundwater model.

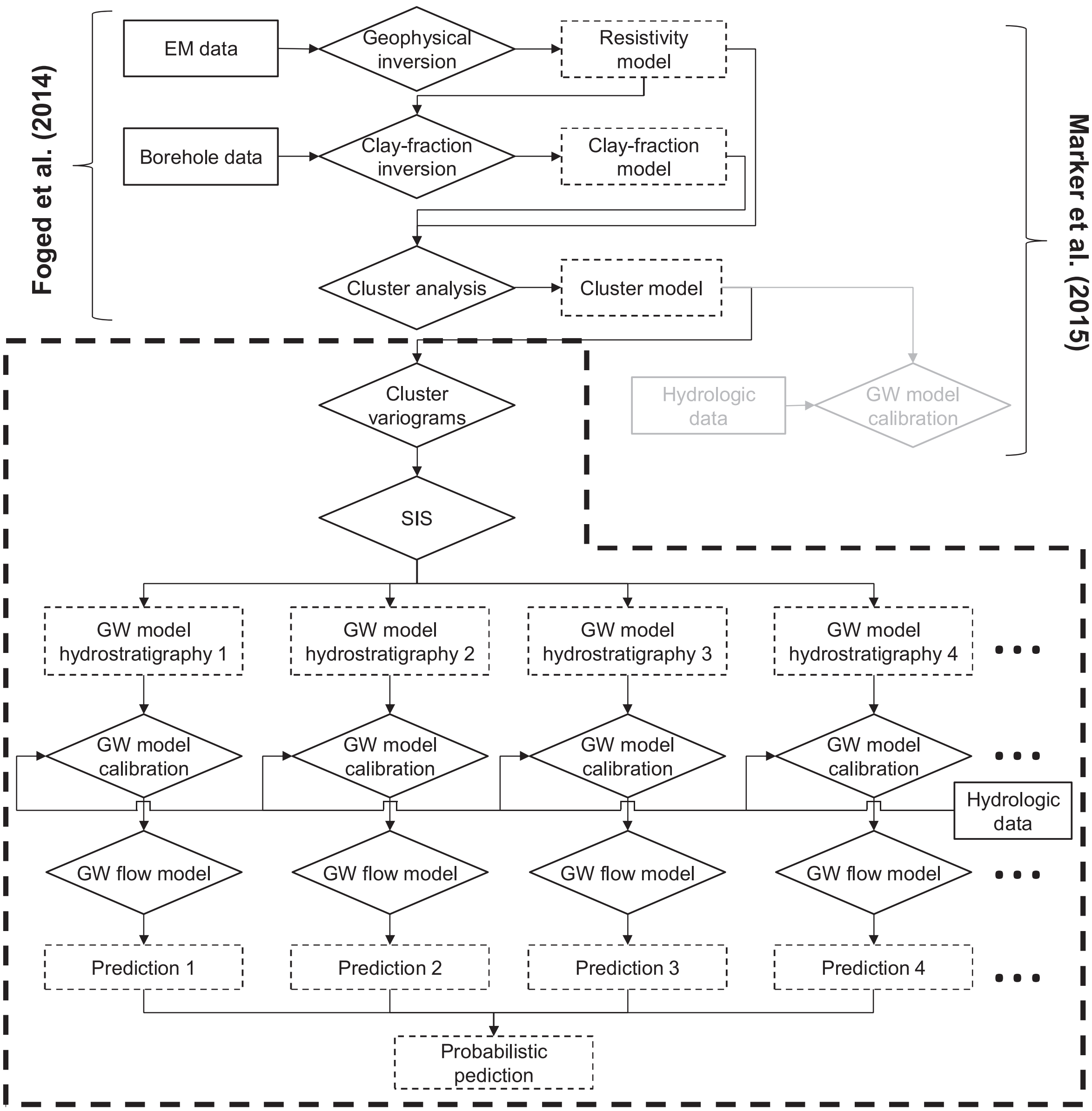

Fig. 1. Overview of complete hydrogeological inversion approach. Square black-lined boxes are input data, square dash-lined boxes are model or model outputs, and diamond shaped boxes represent inversion or other processing steps. The two braces show where details on the first parts of the workflow can be found. The area indicated by the thick black dashed box is the extension of the method, which is the focus of this paper.

2.1. Study area

Throughout this paper we will refer to three areas used in the analysis: the regional area, the local area, and the focus area. The regional area (pink dashed line in Fig. 2) presents the outer limits of the groundwater model and provides the hydrological boundary conditions for the embedded local area model. The ensemble is only created for the local area (thick black line in Fig. 2), which is the target area of the method presented in this paper. Finally the probabilistic prediction results will be shown for a well in the focus area (solid grey line in Fig. 2). Although emphasis is on the local area, the data input to and model setup for the regional and local areas are presented together in Sections 2.2 to 2.6. The methods presented in Section 2.7 (hydrostratigraphic cluster ensemble) are only applied to and presented for the local area.

The regional study area covers 472 km^2 with a local area of 45 km^2, and is located in the eastern part of Jutland, Denmark, see Fig. 2. Quaternary glacial activity has formed the near-surface geological features and current aquifer systems of the study area. The Quaternary sediments were deposited as a consequence of movements of advancing/retreating glaciers from the North/Northeast, and melt-water sediments were incised into the underlying thick Paleogene clays. The incised sediments make up a system of tunnel valleys, which are oriented in several directions due to the omnidirectional glaciations during the Pleistocene. Terrain elevation is up to 126 mamsl (meters above mean sea level) and the 1990–2011 period average annual precipitation is 806 mm. The local area borders the second largest city in Denmark, Aarhus, with a population of approximately 0.3 million people. Groundwater resources are abstracted for drinking water supply. The largest well field (the Kasted well field) has 12 pumping wells located in the center of the local area with a total abstraction between 2 and 3 million m^3/year.

A geological model of the local area is presented by Høyer et al. (2015). The model is based on a manual interpreta-

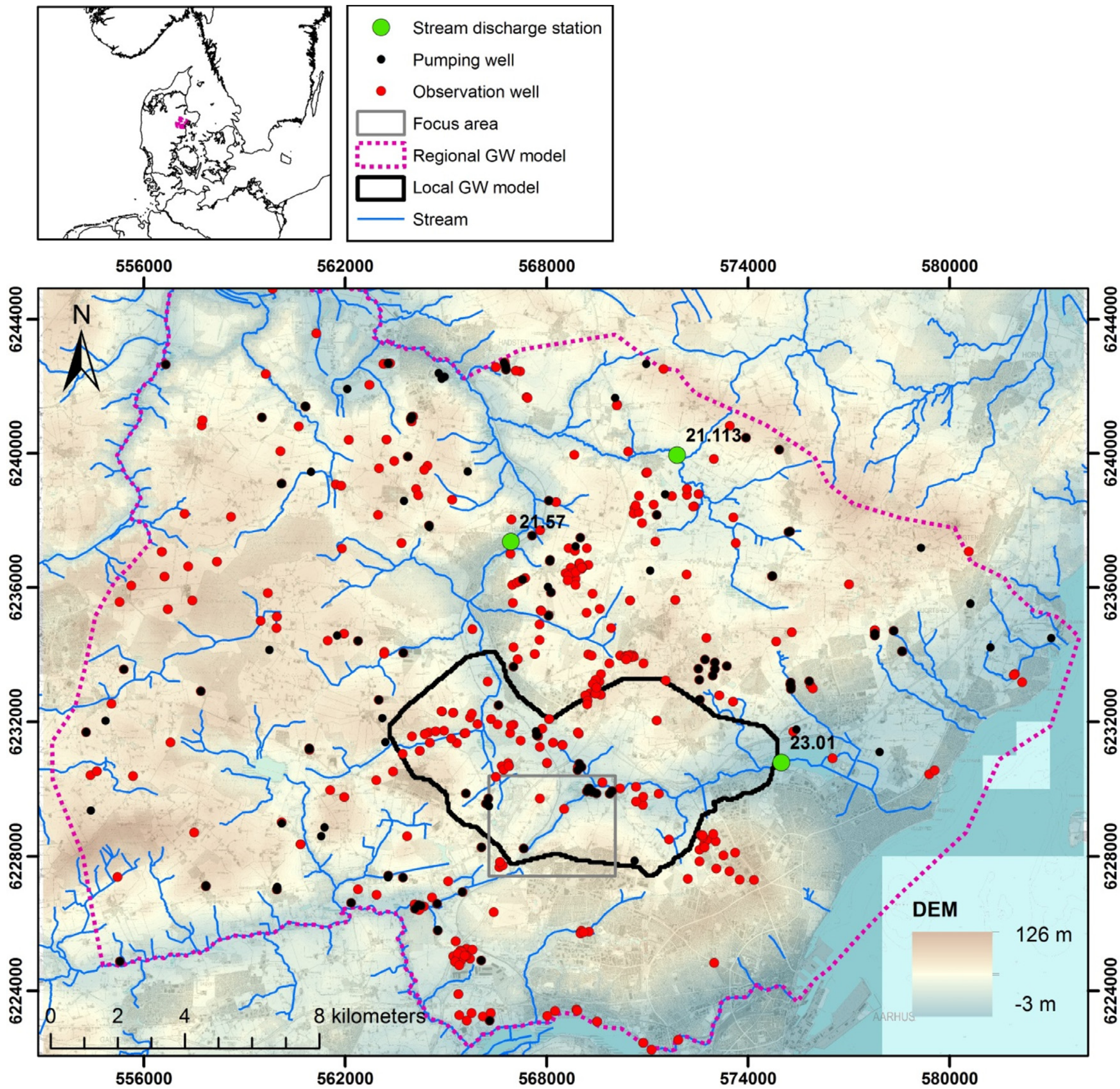

Fig. 2. Basemap of hydrological observations at the Kasted site. The delineation of the regional groundwater model is in dashed pink and the delineation of the local groundwater model is indicated with a bold black line. Head observation wells are marked with red dots, pumping wells with black dots, and the three stream discharge stations are marked with green dots. The catchment area of the discharge station 23.01 falls almost entirely within the local model area. (For interpretation of the references to color in this figure legend, the reader is referred to the web version of this article.)

tion of the same resistivity models and borehole information as the hydrostratigraphical cluster models presented in this paper.

2.2. Geophysical data and inversion

The AEM survey of the local area was conducted in August 2013 with the SkyTEM304 system Sørensen and Auken (2004), where approximately 330 line kilometers were flown with a dense line spacing of 100 m. The resistivity model spacing along the flight lines is approximately 25 m. The SkyTEM data was carefully processed using the Aarhus Workbench software package following the processing scheme described by Auken et al. (2009). During the processing phase data affected by noise (due to coupling to man-made installations and conductors) were removed. The resulting data positions and the subsequent 1D-resistivity model positions are shown in Fig. 3a. The inversion was carried out in a spatially constrained inversion setup (Viezzoli et al., 2008) with a 1D sharp model formulation (Viezzoli et al., 2008), using the AarhusInv inversion code (Auken et al., 2014). In a spatially constrained inversion, a stratified geological environment is mimicked through horizontal and vertical regularization constraints between neighboring 1-D resistivity models. The sharp formulation ensures that vertical transition between contrasting resistivity layers occurring over short vertical distances is rewarded in the inversion objective function, and that smooth vertical transitions are punished. The resistivity models have been terminated individually at their estimated depth of investigation (DOI) calculated as described by Christiansen and Auken (2012). The resistivity values used in the cluster analysis are average resistivity values of fixed elevation intervals. These average resistivity values are obtained by upscaling the resistivity model values, which are obtained through inversion of the geophysical data. See Foged et al. (2014) for details on how the resistivity models have been upscaled.

The geophysical data in the regional area consists of mainly ground based TEM and DC (direct current, a ground based geophysical resistivity method) data collected during the 1990 s, and a minor SkyTEM survey from 2003. In total, the regional area comprises approximately 3,000 ground based single site TEM, 7,400 pulled array TEM (PATEM (Sørensen et al., 2005)), 24,600 SkyTEM, and 225,000 pulled array continuous electrical sounding (PACES) (Sørensen, 1996) resistivity models.

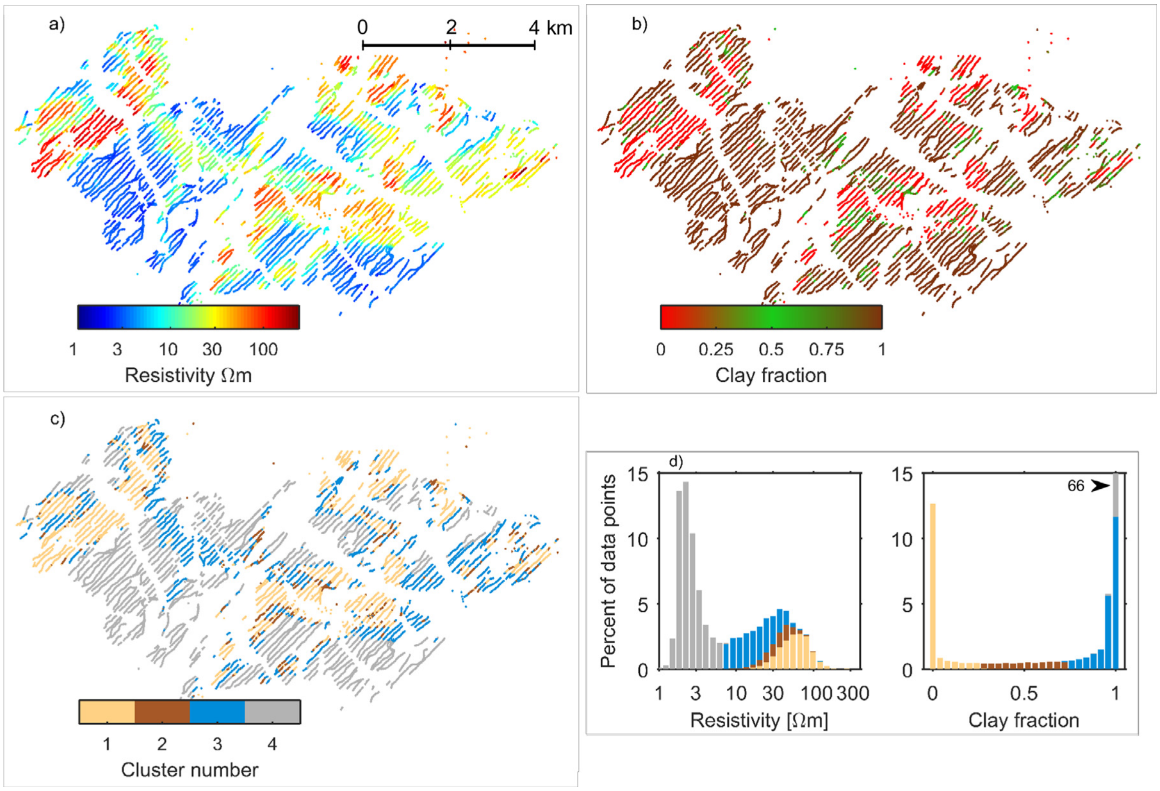

Fig. 3. Cluster variables and cluster model at −2.5 mamsl. a) Resistivity models, b) Corresponding clay-fraction values, c) Corresponding 4 cluster mode model, and d) Histograms of how resistivity and clay fraction values are represented by the clusters.

2.3. Borehole data and clay-fraction procedure

Approximately 400 borehole logs are available in the local model area. 63% or these boreholes are less than 35 m deep and only 3% are deeper than 100 m. Borehole descriptions, locations, and drill depths for the local area can be found in Høyer et al. (2015). Approximately 3000 boreholes are available for the regional area with a similar drill depth distribution as the local area.

The clay-fraction procedure is an inversion approach for spatially variable translation of resistivity values into clay-fraction values, as described by Foged et al. (2014). Observations of sand and clay from borehole logs are used as observations in the inversion. Clay-fraction values, observed and simulated, are defined in fixed elevation intervals, meaning that a clay-fraction value is the accumulated amount of clay in an elevation interval. The translation is carried out by a two-parameter translator function that is allowed to vary in the 3-D model grid. The observations are obtained through interpretation of lithological borehole logs: clayey tills and fat clays for example are interpreted as ‘clay’, while sand and gravel at varying coarseness are interpreted as ‘sand’ . The misfit between simulated and observed clay-fraction values at each elevation interval along with regularization terms in the form of spatial constraints make up the objective function that guides the inversion. Fig. 3b shows the resulting clay-fraction values of the translated resistivity values in Fig. 3a.

2.4. Hydrological data

Base-flow estimates were obtained from three sub-catchments (Fig. 2), and their averaged base flows were utilized in the steady state inversion of the hydrological model. Average base flows are estimated using the automatic filter approach presented by Arnold and Allen (1999) and Arnold et al. (1995).

Steady state hydraulic heads were obtained from a total of 506 measurements within the regional model area (see definition in Fig. 2). 106 of these measurements were collected in the 62 wells that are screened in multiple aquifers, while 336 wells have a single screening interval and thus a single steady state head estimate. Within the local groundwater model area, a total of 94 measurements were available. 19 of the measurements were collected from the 11 wells that are screened at multiple depths, while 75 of the wells have a single screening interval. Uncertainty of each head estimate was evaluated taking into account factors such as: the source of position coordinates (GPS, topographic map etc.); the method used to determine the reference level of a borehole; the length and temporal variation of time series used for estimating steady state heads; and the quality of the borehole (ranging from boreholes being part of the national groundwater monitoring program to old wells used for single household water supply). The estimated errors on observed head range between 2 m and 5 m, please see Henriksen and Sonnenborg (2005) and Appendix A in Marker et al. (2015) for details on the method.

2.5. Groundwater model and calibration

The groundwater model is a steady-state MODFLOW-USG (Panday et al., 2015) model with the 50 m discretized local area embedded in the 100 m discretized regional are (see Fig. 2 for delineations). MODFLOW-USG is a control volume finite difference formulation of the well-known groundwater flow model code MODFLOW (Harbaugh, 2005). No-flow boundaries and constant head boundaries are defined for in-land and sea boundaries respectively. The model is forced by spatially variable recharge. Streams interact with the groundwater through a conductance parameter, which is also spatially variable. Recharge and conductance estimates are obtained by scaling the values used in the Danish national water resources model (Henriksen et al., 2003). Drains are defined throughout the domain and are represented by two conductance values; one for local area and one for the regional area thus accounting for the different grid cell sizes. Stream discharge is calculated as the sum of water drained by drains and the groundwater lost to the streams. Three stream catchments are defined for the regional model area.

The groundwater model calibration is performed using the local non-linear least-squares method implemented in PEST (Doherty J., 2010). The inversion minimizes the misfit, Φ, between simulated head and base flow, h_{sim}, q_{sim}, and observed head and base flow, h_{obs}, q_{obs}, defined as:

$$\Phi = \sum_{i=1}^{N_h} w_i((h_{sim,i} - h_{obs,i})/\sigma_{h,i})^2 + \sum_{i=1}^{N_q} ((q_{sim,i} - q_{obs,i})/\sigma_{q,i})^2 \quad (1)$$

Contributions are weighted according to estimates of observation variances, σ^2. The procedure for estimating the variance (error) on head observations is described in Section 2.4. Observation correlations are not considered, because these are not trivial to determine. To account for overrepresentation of wells in some areas, wells located in areas with a large number of wells have been assigned a lower weight, w_i.

Initially the entire model domain (regional and local area) is calibrated. The hydrostratigraphy for this calibration is built using the *k*-means cluster approach by Marker et al. (2015). All available resistivity models and clay-fraction models for the local and regional areas are used for the subsurface clustering. The calibration utilizes all head observations in the study area and base-flow estimates calculated from the three stream discharge stations, respectively red dots and green dots in Fig. 2. Calibration parameters are horizontal hydraulic conductivity of each cluster, a multiplier of the spatially variable stream bed leakage, and a recharge multiplier of spatially variable recharge estimate. Anisotropy of 1/10 was fixed between horizontal and vertical hydraulic conductivity values. From the calibration of the regional model an average recharge was estimated to 282 mm/year (the yearly precipitation is 806 mm/year), which is reasonable compared to recharge estimates presented by Henriksen et al. (2003), and the estimated 285 mm/yr obtained using an integrated hydrological model in a previous analysis of the groundwater resources, which is presented in a report by Søndergaard et al. (2004). The regionally calibrated recharge was fixed for the local model calibration.

For the local area model calibrations the estimated hydraulic parameters of the regional model are fixed. The local calibration utilizes only head observations in the local area and the base-flow estimate for discharge station 23.01 (base-flow estimates for stations 21.57 and 21.113 are also included in the calibration although with small contribution as the weights are lowered). Calibration parameters are horizontal hydraulic conductivity of each cluster and a multiplier of the spatially variable stream bed leakage.

The parsimonious number of clusters to represent the subsurface of the local area groundwater model is determined by calibrating hydraulic conductivities of models containing 1 to 8 clusters, as was done in Marker et al. (2015). Fig. 4 shows the calibration objective function as a function of the number of clusters in a hydrostratigraphic cluster model. ‘1’ is a homogeneous subsurface. The cluster models are generated according to the approach presented in the subsequent Section 2.7 as modes of a given ensemble. For cluster models with 4 or more clusters the hydraulic properties of the ‘last cluster’ are fixed at values corresponding to impermeable clay (thus representing the Paleogene clay underlying Quaternary deposits, see study area description). With only one degree of freedom difference between the 2-cluster and the 4-cluster model combined with more than 10% decrease in the objective function, the 4-cluster model was selected as the parsimonious model.

As the subsurface is divided into an increasing number of clusters, not only are new hydrostratigraphic interfaces introduced but also existing interfaces are modified. This may explain the poorer fit of the 3-cluster model in comparison to the 2-cluster model, as seen in Fig. 4. The estimated K values of the 2-cluster, 3-cluster and 4-cluster models are presented in Table 1. K2 in the 3-cluster model coincides spatially with K1 and K2 in the 2-cluster model and with K2 and K3 in the 4-cluster model. However, in terms of K value, K2 in the 3-cluster model is similar to K2 in the 2-cluster model and K3 in the 4-cluster model. I.e. the areas/parts of K2 in the 3-cluster model that spatially coincide with K1 in the 2-cluster model and K2 in the 4-cluster model are represented with an inappropriate K value. This indicates that the relatively poorer fit of the 3-cluster model is likely due to a hydrologically unfavorable subdivision of the subsurface. Some parts of the domain, which have a high hydraulic conductivity, have been grouped with other parts, which have a low hydraulic conductivity.

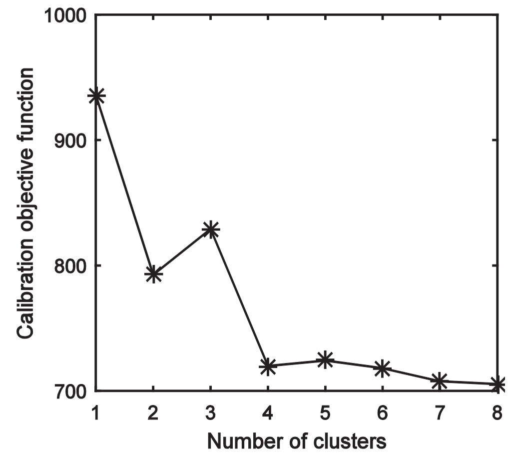

Fig. 4. Parsimonious cluster model selection. Local area groundwater model calibration performance as a function of number of cluster to represent the subsurface, ranging from a homogeneous subsurface (1) to an 8-cluster model (8).

Table 1
Estimated K values in md^{-1} of the clusters in 2-cluster, 3-cluster and 4-cluster models.

	K1	K2	K3	K4
2-cl. model	4.8	3.1×10^{-2}		
3-cl. model	6.0	4.6×10^{-2}	2.9×10^{-2}	
4-cl. model	6.6	3.6	$1.3\cdot10^{-2}$	8.6×10^{-5}*

* *Value fixed during calibration*

2.6. Particle tracking

The uncertainty of a well catchment area was estimated using particle tracking as implemented in mod-PATH3DU (Muffels et al., 2014). A catchment area was estimated using backward tracking. Particles were released from the computational layer where the pumping well is screened. The particles are placed randomly inside a cylinder with a diameter of 25 m and a length corresponding to the computational layer thickness. The particles were tracked backward until termination at the ground surface. The catchment area was subsequently estimated by locating particles that terminated within cells of a 50 m by 50 m grid on the surface. Each cell on the surface thereby contributed to the well catchment if a minimum of one particle terminated within it. Due to computational limitations, the number of particles released was limited to 10,000. To secure model mass balance, the size of the well catchment area must be adjusted, such that the amount of recharge within the catchment corresponds to the amount of water abstracted from the well. The size and the shape of the seeding volume were adjusted by performing a mass balance check on the estimated catchment area, until a reasonable discrepancy was obtained. This seeding volume was then used for the remaining analysis. Well catchment probabilities were estimated by averaging over catchments estimated using all realizations of the input hydrostratigraphy.

2.7. Ensemble of hydrostratigraphic cluster models

An ensemble of equally probable hydrostratigraphical models for the local area is built. The resistivity values and the clay-fraction values form the basis for the ensemble of structural models. The principal components of the spatially coinciding resistivity values and clay-fraction values are subsequently grouped into clusters in a k-means cluster analysis. This approach is presented in Marker et al. (2015). In this paper, the cluster analysis differs from the approach presented in Marker et al. (2015) in two ways: a) the cluster analysis is performed at the geophysical sounding sites at the regular elevation intervals defined in the clay-fraction procedure (i.e. the cluster analysis is carried out in 3-D for the entire domain and the input variables are scattered in xy and regularly distributed in z) and b) clusters are simulated (not kriged) onto a regular grid. The changes made to the approach remove smoothing effects that originate from kriging resistivity values and clay-fraction values. A 5 m depth interval at −2.5 mamsl of the 4-cluster mode model is shown in Fig. 3c. Fig. 3d illustrates how the clusters are represented in terms of resistivity values and clay-fraction values. The clusters are sorted by average corresponding clay-fraction value, i.e. cluster 1 has the lowest clay-fraction value and cluster 4 has the largest clay-fraction value, which is also clear from Fig. 3d. Clusters 1 and 2 have low clay-fraction values and are discriminated by the clay-fraction information while they cannot be discriminated from resistivity values. Clusters 3 and 4 predominantly have clay-fraction values of 1 while the two clusters are clearly different in terms of resistivity values. Cluster 4 is well-defined with resistivity values below 10 Ωm and represents the thick Paleogene clays into which the tunnel valley aquifer systems, of contrasting resistive material, are incised. The resistivity values of Paleogene clays of Danish buried valley systems have been reported in previous studies: Jørgensen et al. (2003a) report values between 1 Ωm and 12 Ωm; Jørgensen et al. (2003b) present values between 1 Ωm and 10 Ωm; and Høyer et al. (2015) reports values below 12 Ωm.

The ensemble of cluster models is generated as realizations utilizing sequential indicator simulation (SIS) (Gómez-Hernández and Srivastava, 1990). The sequential indicator simulation code, SISIM, from the geostatistical package GSLIB (Deutsch and Journel, 1998) was used. The algorithm simulates scattered categorical data onto a regular grid using a variogram model for each category. The probability of occurrence of a category separated by a distance h is described by its sample indicator semi variance $\gamma_s(h)$:

$$\gamma_s(h) = 1/(2N(h)) \sum_{i}^{N(h)} (I(i) - I(i+h))^2 \quad (2)$$

where $I(i)$ is the indicator value at point i and $N(h)$ is the number of observation pairs for the separation distance h. I.e. the indicator variogram value $2\gamma_s(h)$ measures how often two locations a distance h apart belong to different categories [47, p35 Goovaerts (1997)].

In terms of the xy plane, the SIS simulation grid and the numerical groundwater model layers are the same. The SIS grid however is discretized into regular 5 m intervals in the vertical, whereas the numerical groundwater model consists of 11 layers of varying thickness. The upscaling from the SIS grid to the numerical groundwater model layers is handled using the MODFLOW-USG utility geo2mfusg.exe (Vilhelmsen, 2012), which calculates horizontal and vertical hydraulic conductivities respectively as arithmetic and geometric means.

Using SIS in combination with geophysical data has been demonstrated in Gómez-Hernández and Wen (1994) and

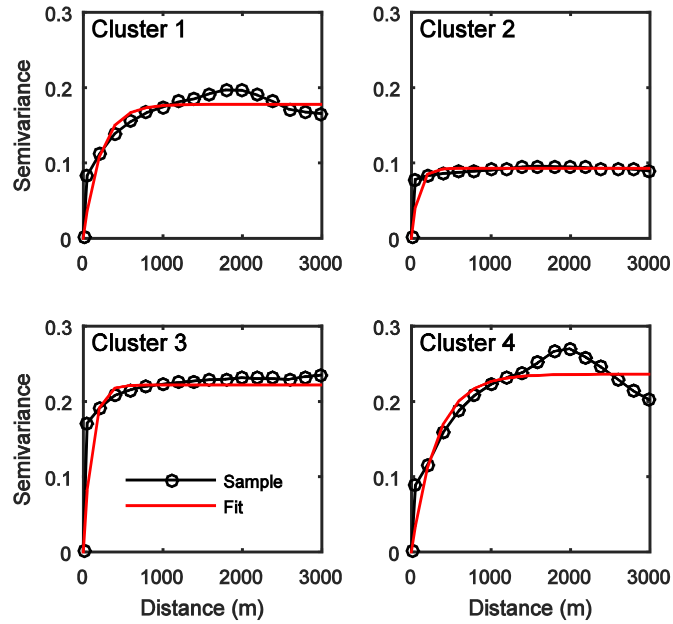

Fig. 5. Horizontal sample and fitted indicator variograms for the four clusters of the 4-cluster model.

Klise et al. (2009). Using geostatistical simulation with geophysical models introduces the issue of over-conditioning if the spatially, especially horizontally, correlated geophysical models are not treated properly (Koch et al., 2014). The method presented in this paper automatically solves this issue by combining geophysical and borehole information into clusters, and performing the simulation on clusters instead of directly on geophysical models.

Contrary to two-point statistics, multiple point statistics (MPS) has the advantage of reproducing realistic geological features, such as channel structures, see review by Linde et al. (2015) and references therein. Due to the dense coverage of AEM data, in which dominating geological features are already captured (for example tunnel valley systems), the simpler two-point statistical SIS approach using variogram models was chosen in this paper. Also MPS, as described for example by Ronayne et al. (2008), is computationally very demanding. Computational resources in this paper were spent on hydrological inversion for a large number of hydrostratigraphic realizations.

Exponential indicator variogram models are fitted to the experimental variograms of each cluster. Fig. 5 shows experimental variograms as well as fitted variogram models for each cluster in the 4-cluster model. Nugget models represent uncertainty in the data or within grid uncertainty as random error. We have not included nugget effects in the modeled variograms because nugget effects would result in random checkerboard patterns in the simulated models, which are not necessarily hydrostratigraphically meaningful. Data uncertainty should represent the uncertainty in the estimated resistivity model values and clay-fraction values. Thus, following the strategy of this paper, data uncertainty must be addressed prior to clustering. This paper has not addressed uncertainty in the estimated resistivity model values and clay-fraction values, although this may be an important component of uncertainty. An automatic variogram fitting routine (Pebesma, 2004) was used to fit the 36 horizontal variogram models (this covers all cluster of the cluster mode models shown in Fig. 4), some of which were inspected manually to verify and check reasonability of the fit. The sill of the corresponding vertical variogram model is the same as the horizontal sill while the range was obtained by scaling the horizontal range by a factor ranging between 10 and 20,

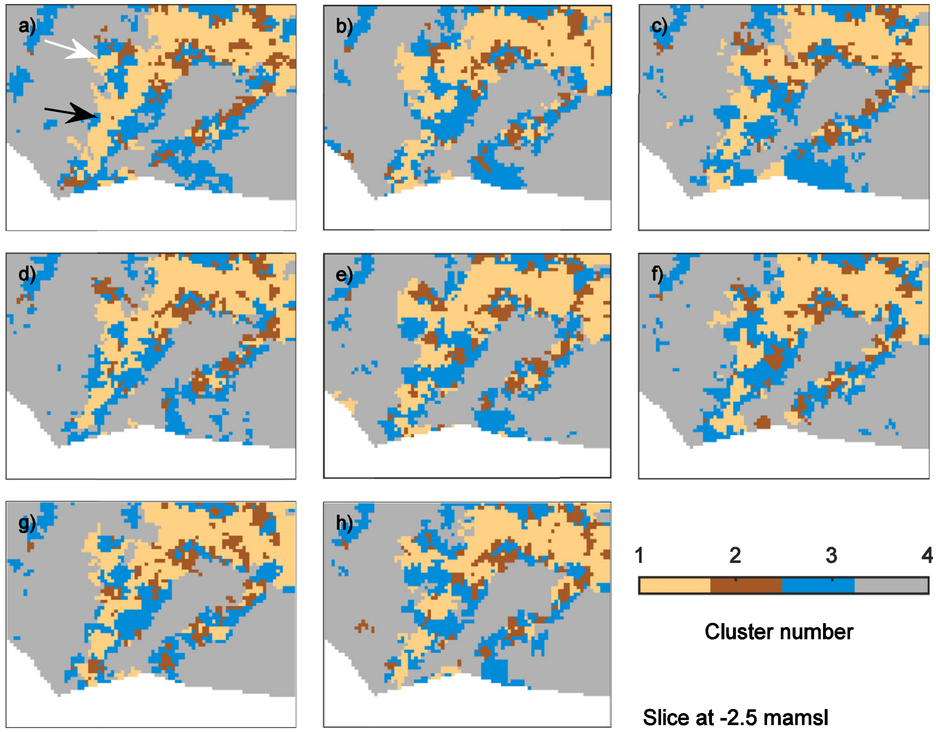

Fig. 6. Eight realizations of the ensemble, shown for a 5 m depth interval at −2.5 mamsl of the focus area. The location of the focus area is shown on Fig. 2.

which was determined from manual inspection. Automatic fitting routines for variograms do not necessarily guarantee best representation of spatial properties (length mean, length standard deviation, and proportion) of the categories, nor that the correct model structure has been chosen (Ritzi, 2000). Because we do not explicitly interpret the characteristics of the clusters (in terms of geology, lithology or hydrostratigraphy), a manual selection of a variogram model based on background knowledge about the spatial behavior of the modeled phenomenon is in this case not straightforward.

The ensemble of structure models thus captures the uncertainty originating from incomplete data coverage. Resistivity values and clay-fractions value are used deterministically and the stochastic models are generated as realizations to fill out gaps in the data coverage.

3. Results and discussion

The hydrological analysis is based on 75 realizations of hydrostratigraphical cluster models. Other studies that report hydrological models and analyses based on geostatistically generated subsurface realizations have used ensembles with a number of realizations ranging from 10 to 200 (Gómez-Hernández, 1994; Gunnink and Siemon, 2015; He et al., 2015; Goovaerts, 1999). Realizations of the subsurface structures will be shown for the focus area. Particle tracking will be considered for pumping well 89.1221, which is located in the Kasted well field (Fig. 11).

The uncertainty of hydrological predictions originating from subsurface structural uncertainty is assessed through the prediction of the well catchment area for pumping well 89.1221. The result does not represent an average level of uncertainty for this type of prediction; the calculated uncertainty is valid for the selected well only.

3.1. Ensemble realizations

A horizontal slice of the focus area at −2.5 mamsl for 8 realizations is shown in Fig. 6a-h. A relatively large part of the focus area is not covered by AEM data. The realizations show variation in the simulated structure of a SW-NE trending valley (black arrow in Fig. 6a). The valley is either connected or disconnected with cluster 1 (in 2-D as shown here). The presence of a valley however is represented throughout the 75 realizations; the variability simulated using the indicator variograms thus represents fine scale features. Although cluster 1 has the largest variogram range and sill values, cluster 1 is interrupted by cluster 2 and cluster 3. Cluster 2 is more discontinuous in space, which is also clear from the variogram. The composition of the valley fill with respect to cluster 1, cluster 2, and cluster 3 and the area marked by the white arrow in Fig. 6a varies throughout the realizations. Although the effective hydraulic connectivity of the entire valley in three dimensions might not vary between realizations, local flow patterns are likely to differ due to differences in spatial orientation of cluster 1, cluster 2, and cluster 3. Apart from groups of boreholes at the corners of the focus area, borehole information in the focus area includes 3 boreholes of 40 to 80 m depth and 4 boreholes of 15 to 40 m depth, and the remaining boreholes are shallow wells between 0 and 15 m depth. See Høyer et al. (2015) for a map of the boreholes.

The hydrological and geological interpretation of geophysical resistivity models is known to be non-unique, because formation resistivity depends on both lithology and porewater quality, see for example Barfod et al. (2016) and Purvance and Andricevic (2000). This issue must be considered in any hydrogeological application of geophysical data or models. In a manual geological model building process, a modeler depends on borehole information to interpret the geophysical models. In the cluster approach, borehole information is incorporated through the clay-fraction procedure. When lithological information is available, the clay-fraction value is fixed for the given location. Fig. 3d shows an example of this. Clusters 1 and 2 overlap entirely with respect to resistivity values, while clusters 1 and 2 are clearly separated with respect to clay-fraction values. To resolve non-uniqueness the model parameters in the translator function will be adjusted in order to translate the resistivity model into a clay-fraction value similar to the observed. In areas

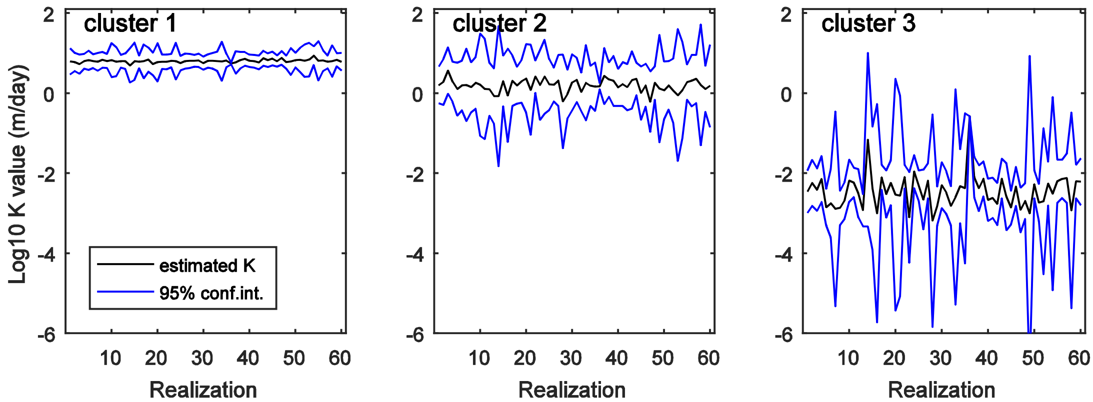

Fig. 7. Estimated hydraulic conductivity values (black lines) for 60 of the 75 calibrated models and associated 95% confidence intervals (blue lines). (For interpretation of the references to colour in this figure legend, the reader is referred to the web version of this article.)

with little or no borehole information, it is difficult to correctly attribute resistivity variations to lithology/porewater quality variations. This naturally applies for cognitive as well as automatic approaches. However, little variation of pore-water quality has been reported for the Kasted area (Søndergaard et al., 2004).

The cluster approach is here presented for a geological setting where the main aquifer structures are determined by the distribution of sand, gravel, till, and clay sediments. We are able to map these structures with EM methods and we can use the clay-fraction procedure to handle non-uniqueness related to the distribution of sand/clay sediments. The method presented in this paper may not be directly transferable to different geological settings, for example fractured limestone aquifers.

3.2. Results of local calibration

The calibrated hydraulic conductivity values of the clusters are 5.2 to 7.0 md^{-1}, 0.85 to 3.5 md^{-1} and 8.6 10^{-4} to 6.9 10^{-3} md^{-1} for cluster 1, cluster 2, and cluster 3 respectively. The estimated K values and the corresponding 95% confidence intervals for 60 out of the 75 realizations are presented in Fig. 7. It was only possible to calculate parameter covariance matrices for 60 realizations.

The RMSE and ME of simulated head and the percentage error of simulated base flow at station 23.01 for the 75 realizations is displayed in Fig. 8. RMSE values (black line) fluctuate around 5.5 m and ME values (blue line) fluctuate around 0 m, with the exception of a few outliers. The misfit for base flow (red line) is between 0% and −4% for the majority of the realizations.

Calibration results with respect to head are shown in Fig. 9b with a scatter plot of observed versus simulated hydraulic head. The median of the 75 realizations is illustrated with a red cross and the minimum and maximum values are illustrated with the black vertical lines. The blue dashed lines indicate a 5 m misfit to observed heads.

Fig. 9a shows a map of the absolute median and standard deviation of the misfits of the 75 calibrated models. Red, yellow and green dots are observations associated with a low to intermediate median misfit. Light and dark blue dots overlapping with small grey dots (small standard deviation) indicate observations that are not fitted well throughout the ensemble.

Observation A, see Fig. 9a, is located in an area with little AEM data, but the borehole is deep and there is thus lithological information. The ensemble is constrained by lithological information in this area, which explains the agreement between the realizations. The borehole is one out of two deep wells in the area, which is otherwise represented by shallow boreholes between 0 and 15 m depths. The large misfit of A may therefore be due to the lack of surrounding structural information, and thus an uncertain structural representation of the area. The observations in group B in Fig. 9a have a low weight in the groundwater calibration. This can explain why the realizations fail to fit these observations, despite of good AEM and borehole coverage in the area. The observations in group C are found in an area with a good AEM and borehole coverage. The biased misfit in the realizations is potentially related to structures misinterpreted or unaccounted for in the model.

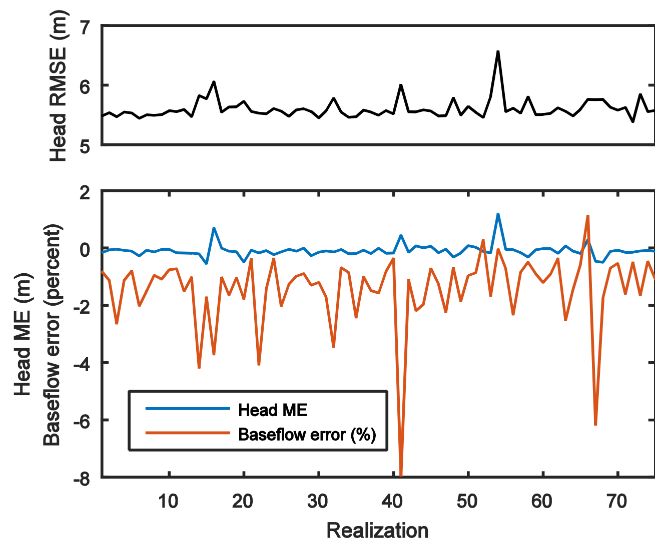

Fig. 8. RMSE and ME for head and percentage misfit for base flow. The black line in the uppermost panel shows RMSE in meters; in the lower panel the blue line is ME in meters and the misfit for base flow in % is shown with the red line. (For interpretation of the references to colour in this figure legend, the reader is referred to the web version of this article.)

3.3. Well catchment area predictions

Convergence of the probabilistic catchment area as a function of the number of realizations is illustrated Fig. 10.

Fig. 11 shows the probabilistic well catchment area of well 89.1221 based on the 75 hydrostratigraphic realizations. The map is produced by generating a binary grid map (50 m by 50 m grid size) for each realization; 1 indicates that one or more particles reach the grid cell, and 0 indicates that no particles reach the grid cell. The 75 binary grid maps are combined in a 2-D histogram. The map is normalized to express occurrence frequency where 1 is 100% and 0 is 0%. Colors of the probabilistic catchment correspond approximately to: light blue 85% (64 out of 75 realizations); cyan 63% (47 out of 75 realizations); yellow 30% (25 out of 75 realiza-

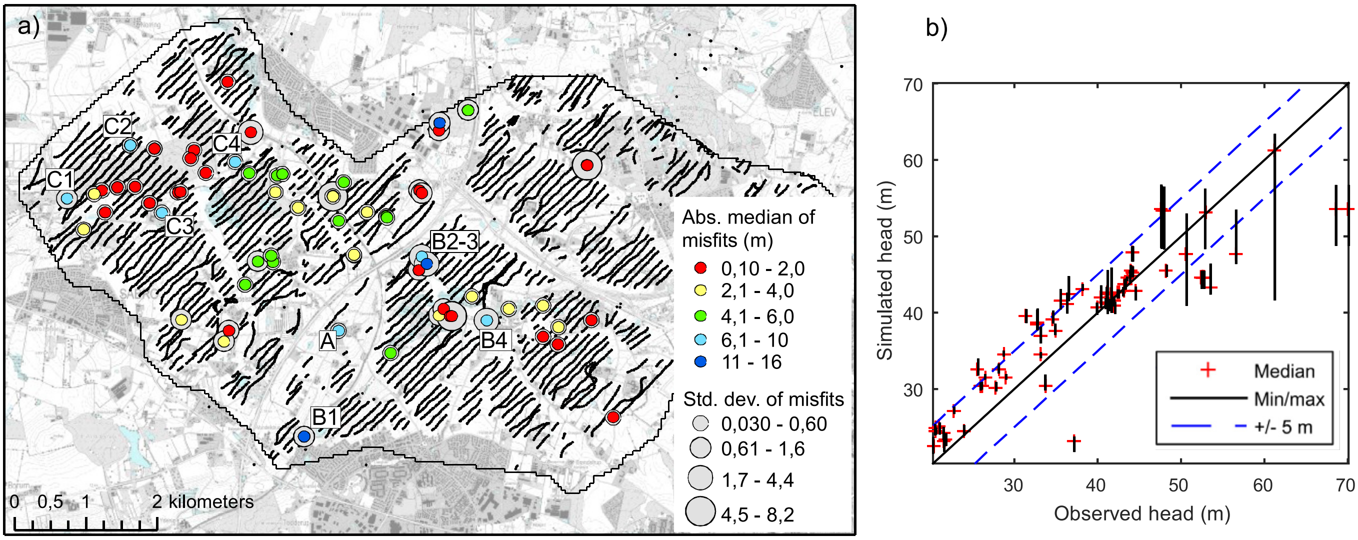

Fig. 9. a) Map of the absolute median misfit and standard deviation of the ensemble, b) Simulated versus observed hydraulic head.

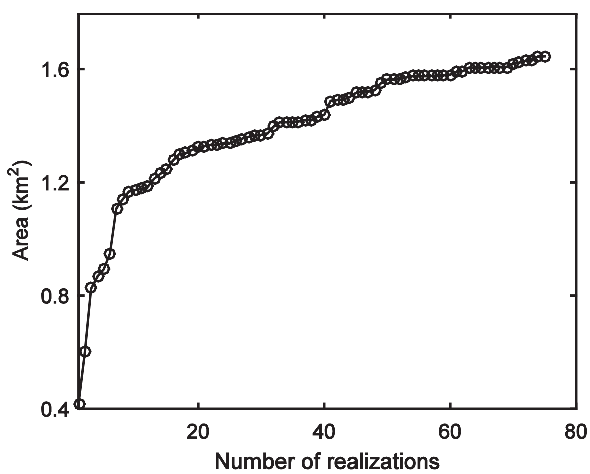

Fig. 10. Area covered by probabilistic catchment area for well 89.1221 as a function the number of realizations.

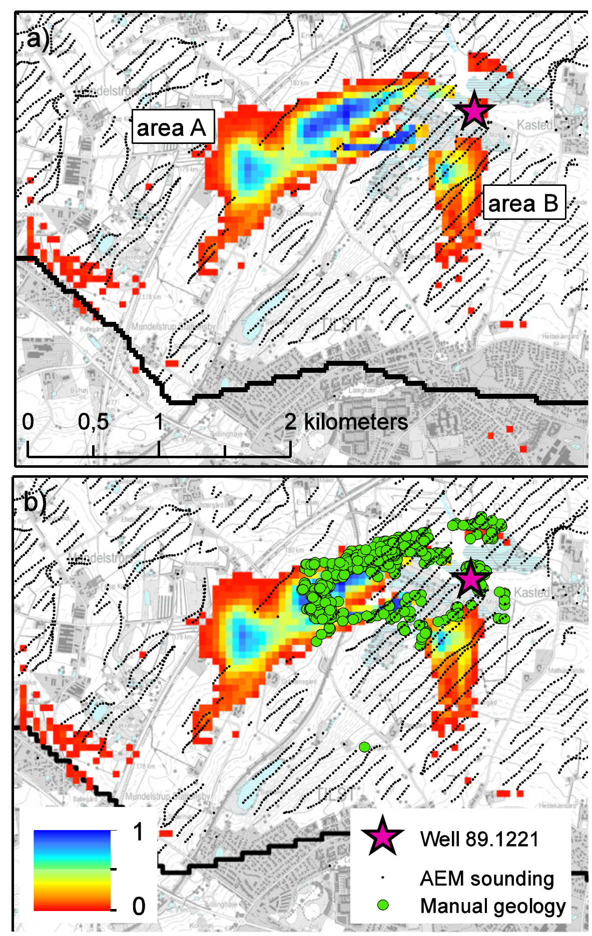

Fig. 11. Probabilistic catchment area for pumping well 89.1221. The star indicates the location of the pumping well. Green dots are the particle endpoint locations obtained with the manual geological model. Black dots are AEM sounding sites. (For interpretation of the references to color in this figure legend, the reader is referred to the web version of this article.)

tions); orange 15%; red 2% (2 out of 75 realizations). Two realizations contribute to the catchment grid nodes in the area close to the south-western border of the local model area. The initial particle locations, which are determined at random, have insignificant effect on the resulting catchment delineation. This was checked by comparing the probabilistic catchment areas resulting from three sets of random particle starting locations.

A local groundwater model calibration was performed using the manually constructed geology of the local area (Høyer et al., 2015). The resulting well catchment area is shown with green dots in Fig. 11b. The groundwater model and calibration setup, as well as particle tracking routine, used for the manually constructed geology are identical to those used for the cluster ensemble. The manually constructed geology is based on the same borehole information and resistivity models. Aside from added expert knowledge, the geologists processes and interprets the borehole information and resistivity models in a manner very different from that of the automatic clustering routine. We therefore use the well catchment area predicted with the groundwater model informed with the manually constructed geology as a bias check for the ensemble predictions.

64 out of the 75 realizations predict that the well catchment area includes area A, see Fig. 11. This area is not included in the well catchment area, when the manually constructed geology is used to predict the well catchment area. Borehole information in the well catchment area is very limited. Apart from two boreholes that are between 40 to 80 m deep, the few remaining boreholes

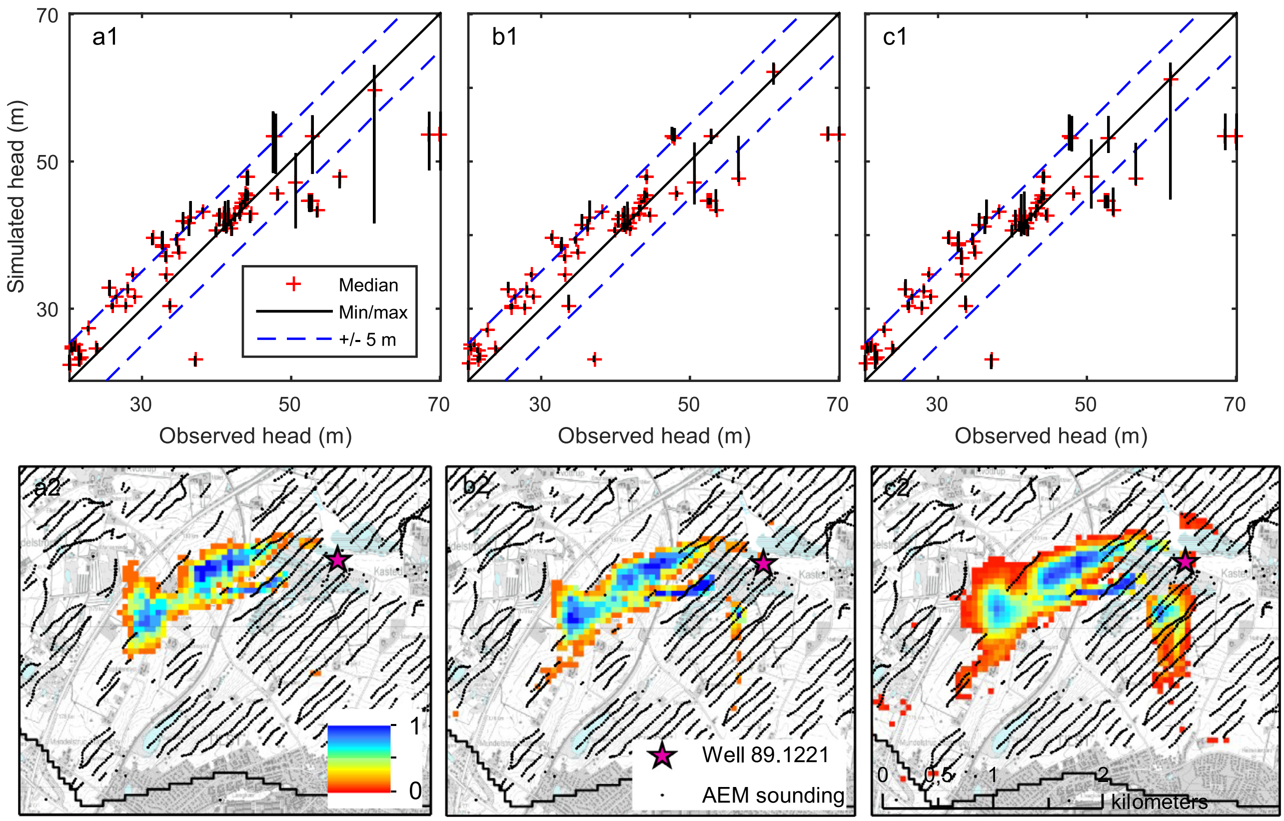

Fig. 12. Head misfits and well catchment prediction for selected groups of realizations. a1), b1) and c1) show head misfits, and a2), b2), and c2) show the corresponding catchment predictions for each of the three groups of realizations.

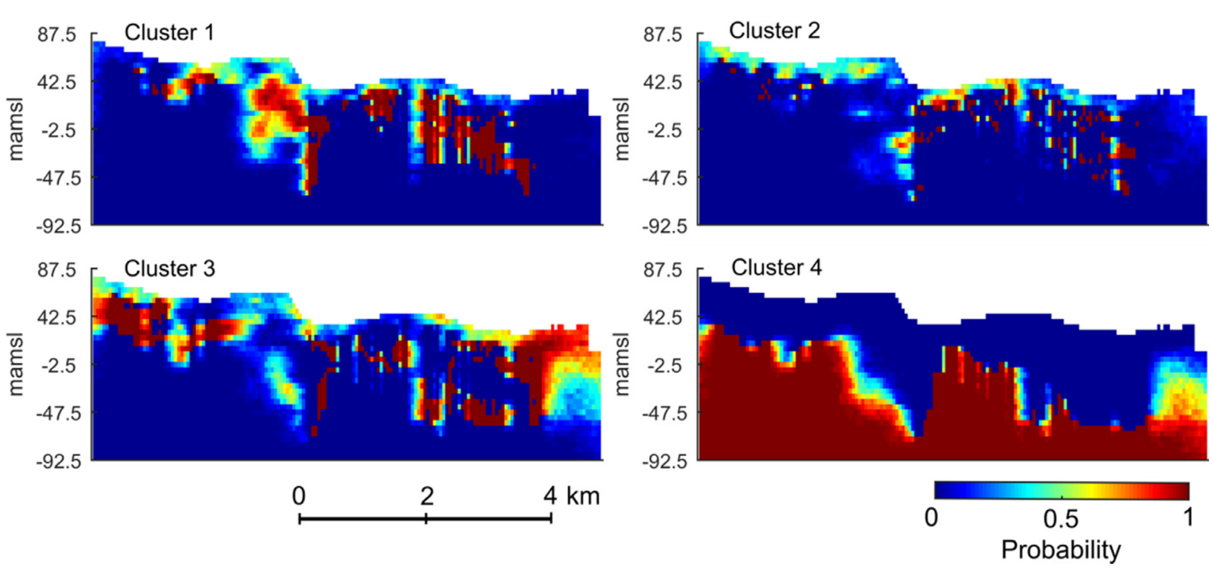

Fig. 13. Probabilistic representations of the four clusters, shown for a cross section through the center of the entire domain. The profile is oriented W-E. A value of 1 indicates that the grid cell belongs to the given cluster across all 75 realizations.

in the area are between 0 to 15 m deep (see Fig. 1 in Høyer et al., 2015). AEM data in the area is missing too due the local noise conditions. Thus, the spatial orientation of aquifer material is uncertain in this part of the domain. Area B is also not predicted by the manual geology. This area, although covered with AEM data, has no borehole information to interpret the lithology.

Nine realizations do not predict any particles for area B, while another ten realizations predict only a few particles (or grid cells) for area B.

Fig. 12 shows head misfits (1) and predicted catchment area (2) for three groups of realizations. Fig. 12a is the group of nine realizations that do not predict the well catchment to area B, Fig. 12b is the group of ten realizations that predict a minor part of the well catchment to extend to area B, while Fig. 12c is the group of all realizations not including group a and group b. With respect to the overall correspondence between simulated and observed heads, Fig. 12a1 and Fig. 12c1 resemble Fig. 9b the most. Despite of the similarity between group a and group c in terms of simulated hydraulic heads, group a and group c disagree whether the catchment includes area B or not. We cannot discriminate the models in group a and group c in terms of their ability to fit hydraulic head observations, but the two groups shows a clear difference in the predicted catchment area for well 89.1221. This illustrates that two models which have similar calibration performance can produce significantly different predictions.

Fig. 13 shows cluster occurrence probabilities of a W-E trending cross section through the domain at the location of pumping well 89.1221. The panels illustrate cluster 1 to cluster 4. Colors indicate the probability of a cluster occurring in a given grid node across the 75 realizations; given a value 1 (dark red areas) a grid node belongs to the same cluster throughout the 75 realizations. Blurred colors indicate uncertain areas due to data gaps. There is no direct relationship between the uncertainty of the hydrostratigraphic model and the resulting well catchment uncertainty.

4. Conclusions

This paper aims to demonstrate a sequential hydrogeophysical inversion approach to estimate the predictive uncertainty of a groundwater model, which originates from subsurface structural uncertainty. The workflow integrates a large scale AEM dataset and borehole information directly into the hydrological modeling process. The demonstration is based on the delineation of a probabilistic well catchment area. The paper shows an example for an aquifer system in Denmark, which is formed by glacial activity, and results are compared to those obtained from a manually generated geological model. The workflow is a unique and semi-automatic hydrogeophysical approach to structure-dependent hydrological uncertainty estimation.

We generated the ensemble of 75 hydrostratigraphic models using SIS based on indicator variograms of scattered categorical cluster. The clusters were obtained through a k-means cluster analysis on resistivity values (obtained from inversion of AEM data) and clay-fraction values. A 45 km^2 steady-state groundwater model was used for the analysis. Each realization of the ensemble was calibrated separately against observed hydraulic head and baseflow estimates. Overall, hydraulic heads were fitted to an RMSE of 5.5 m and baseflow was fitted to between 0 and −4 percent error.

Because the main geological features (the system of tunnel valley aquifers) are captured in the AEM data, these features are maintained throughout the ensemble of hydrostratigraphical models. The variation between realizations represents disconnection/connection of conductive/impermeable aquifer material at smaller scales. This variation results in predicted well catchment areas that are similar in terms of the overall shape and location, but with large local differences between the realizations. As a result the size of the delineated catchment area depends of the certainty/probability with which the catchment is wished to be delineated. For example, area A is included in the catchment area in 64 out of the 75 realizations. A comparison of three subgroups of the ensemble confirmed that differentiation of realizations in terms of calibration data (head observations) does not reflect variation in the predicted well catchment area between the realizations.

The probabilistic catchment area includes the catchment area that is predicted when the manually constructed geology is used in the groundwater model. The overlap of respectively the deterministic approach and the stochastic approach to model the hydrostratigraphy indicates that the main features of the aquifer systems have been captured by the ensemble. Area A and area B are not included in the well catchment area of the manually generated geology. There is no borehole information in area B. The deterministic model reflects one interpretation of the resistivity models, which results in area B not being included in the catchment area, whereas the ensemble reflects the possibility that the catchment area includes area B.

Acknowledgements

The authors would like to thank the editor and Niklas Linde and two anonymous reviewers for constructive criticism during the review process, which has been of great value to the final outcome. Also we would like to thank Chris Muffels of S.S Papadopulos & Associates Inc. for close communication and support regarding the use of mod-PATH3DU for MODFLOW-USG. This paper was supported by HyGEM, Integrating geophysics, geology, and hydrology for improved groundwater and environmental management, Project no. 11–116763. The funding for HyGEM is provided by The Danish Council for Strategic Research.

References

Arnold, J.G., Allen, P.M., 1999. Automated methods for estimating baseflow and ground water recharge from streamflow records. J. Am. Water Resour. Assoc. 35, 411–424. http://dx.doi.org/10.1111/j.1752-1688.1999.tb03599.x.

Arnold, J.G., Allen, P.M., Muttiah, R., Bernhardt, G., 1995. Automated base flow separation and recession analysis techniques. Ground Water 33, 1010–1018. http://dx.doi.org/10.1111/j.1745-6584.1995.tb00046.x.

Auken, E., Christiansen, A.V., Westergaard, J.H., Kirkegaard, C., Foged, N., Viezzoli, A., 2009. An integrated processing scheme for high-resolution airborne electromagnetic surveys, the SkyTEM system. Explor. Geophys. 40, 184. http://dx.doi.org/10.1071/EG08128.

Auken, E., Christiansen, A.V., Kirkegaard, C., Fiandaca, G., Schamper, C., Behroozmand, A.A., et al., 2014. An overview of a highly versatile forward and stable inverse algorithm for airborne, ground-based and borehole electromagnetic and electric data. Explor. Geophys. http://dx.doi.org/10.1071/EG13097.

Barfod, A.A.S., Møller, I., Christiansen A, V., 2016. Compiling a national resistivity atlas of Denmark based on airborne and ground-based transient electromagnetic data. J. Appl. Geophys. 134, 199–209.

Bosch, J.H.A., Bakker, M.A.J., Gunnink, J.L., Paap, B.F., 2009. Airborne electromagnetic measurements as basis for a 3D geological model of an Elsterian incision
[Hubschrauberelektromagnetische Messungen als Grundlage für das geologische 3*D-Modell einer glazialen Rinne aus der Elsterzeit*]. Zeitschrift Der Dtsch Gesellschaft Für Geowissenschaften 160, 249–258. http://dx.doi.org/10.1127/1860-1804/2009/0160-0258.

Burschil, T., Scheer, W., Kirsch, R., Wiederhold, H., 2012. Compiling geophysical and geological information into a 3-D model of the glacially-affected island of Föhr. Hydrol. Earth Syst. Sci. 16, 3485–3498. http://dx.doi.org/10.5194/hess-16-3485-2012.

Chongo, M., Vest Christiansen, A., Tembo, A., Banda, K.E., Nyambe, I.A., Larsen, F., et al., 2015. Airborne and ground-based transient electromagnetic mapping of groundwater salinity in the Machile–Zambezi Basin, southwestern Zambia. Near. Surf. Geophys. 13, 383–395. http://dx.doi.org/10.3997/1873-0604.2015024.

Christiansen, A.V., Auken, E., 2012. A global measure for depth of investigation. Geophysics 77, WB171–WB177. http://dx.doi.org/10.1190/geo2011-0393.1.

Christiansen, A.V., Foged, N., Auken, E., 2014. A concept for calculating accumulated clay thickness from borehole lithological logs and resistivity models for nitrate vulnerability assessment. J. Appl. Geophys. 108, 69–77. http://dx.doi.org/10.1016/j.jappgeo.2014.06.010.

Delhomme, J.P., 1979. Spatial variability and uncertainty in groundwater flow parameters: a geostatistical approach. Water Resour. Res. 15, 269–280. http://dx.doi.org/10.1029/WR015i002p00269.

Dell'Arciprete, D., Bersezio, R., Felletti, F., Giudici, M., Comunian, A., Renard, P., 2011. Comparison of three geostatistical methods for hydrofacies simulation: a test on alluvial sediments. Hydrogeol. J. 20, 299–311. http://dx.doi.org/10.1007/s10040-011-0808-0.

Deutsch, C., Journel, A.G., 1998. GSLIB: Geostatistical Software Library and User's Guide. Oxford University Press.

Dickson, N.E.M., Comte, J.-C., Renard, P., Straubhaar, J.A., McKinley, J.M., Ofterdinger, U., 2015. Integrating aerial geophysical data in multiple-point statistics simulations to assist groundwater flow models. Hydrogeol J. 23, 883–900. http://dx.doi.org/10.1007/s10040-015-1258-x.

Doherty J., P.E.S.T., 2010. Model-Independent Parameter Estimation Brisbane, QLD, Australia User Manual: 5th Edition.

Foged, N., Marker, P.A., Christansen A, V., Bauer-Gottwein, P., Jørgensen, F., Høyer, A.-S., et al., 2014. Large scale 3-D modeling by integration of resistivity models and borehole data through inversion. Hydrol. Earth Syst. Sci. 18, 4349–4362. http://dx.doi.org/10.5194/hess-18-4349-2014.

Friedel, M.J., de Souza, O.A., Iwashita, F., Silva, A.M., Yoshinaga, S., 2012. Data-driven modeling for groundwater exploration in fractured crystalline terrain, northeast Brazil. Hydrogeol. J. 20, 1061–1080. http://dx.doi.org/10.1007/s10040-012-0855-1.

Gómez-Hernández, J.J., Srivastava, R., 1990. ISIM3D - An ANSI-C 3-dimensional multiple indicator conditional simulation program. Comput. Geosci. 16, 395–440.

Gómez-Hernández, J.J., Wen, X.-H., 1994. Probabilistic assessment of travel times in groundwater modeling. . Stoch. Hydrol. Hydraul. 8, 19–55. http://dx.doi.org/10.1007/BF01581389.

Gondwe, B.R.N., Lerer, S., Stisen, S., Marín, L., Rebolledo-Vieyra, M., Merediz-Alonso, G., et al., 2010. Hydrogeology of the south-eastern Yucatan Peninsula: New insights from water level measurements, geochemistry, geophysics and remote sensing. J. Hydrol. 389, 1–17. http://dx.doi.org/10.1016/j.jhydrol.2010.04.044.

Goovaerts, P., 1997. Geostatistics For Natural Resources Evaluation. Oxford University Press.

Goovaerts, P., 1999. Impact of the simulation algorithm, magnitude of ergodic fluctuations and number of realizations on the spaces of uncertainty of flow properties. Stoch. Environ. Res. Risk Assess 13, 161–182. http://dx.doi.org/10.1007/s004770050037.

Gunnink, J.L., Siemon, B., 2015. Applying airborne electromagnetics in 3D stochastic geohydrological modelling for determining groundwater protection. Near. Surf. Geophys 13, 45–60. http://dx.doi.org/10.3997/1873-0604.2014044.

Høyer, A.-S., Jørgensen, F., Sandersen, P.B.E., Viezzoli, A., Møller, I., 2015. 3D geological modelling of a complex buried-valley network delineated from borehole and AEM data. J. Appl. Geophys. 122, 94–102. http://dx.doi.org/10.1016/j.jappgeo.2015.09.004.

Harbaugh, A.W., 2005. The U.S. Geological Survey Modular Ground-Water Model - the Ground-Water Flow Process. In: U.S. Geological. Survey. Techniques and Methods Reston, Virginia, 6–A16, p. 253.

He, X., Højberg, A.L., Jørgensen, F., Refsgaard, J.C., 2015. Assessing hydrological model predictive uncertainty using stochastically generated geological models. Hydrol. Process 29, 4293–4311. http://dx.doi.org/10.1002/hyp.10488.

Henriksen, H.J., Sonnenborg, T.O., 2005. Nøjagtighedskriterier. GEUS, København:.

Henriksen, H.J., Troldborg, L., Nyegaard, P., Sonnenborg, T.O., Refsgaard, J.C., Madsen, B., 2003. Methodology for construction, calibration and validation of a national hydrological model for Denmark. J. Hydrol. 280, 52–71. http://dx.doi.org/10.1016/S0022-1694(03)00186-0.

Hermans, T., Nguyen, F., Caers, J., 2015. Uncertainty in training image-based inversion of hydraulic head data constrained to ERT data: Workflow and case study. Water Resour. Res. 51, 5332–5352. http://dx.doi.org/10.1002/2014WR016460.

Hinnell, A.C., Ferre, T.P.A., Vrugt, J.A., Huisman, J.A., Moysey, S., Rings, J., et al., 2010. Improved extraction of hydrologic information from geophysical data through coupled hydrogeophysical inversion. Water. Resour. Res. 46. http://dx.doi.org/10.1029/2008wr007060, W00D40.

Jørgensen, F., Sandersen, P.B.E., Auken, E., 2003a. Imaging buried Quaternary valleys using the transient electromagnetic method. J. Appl. Geophys. 53, 199–213. http://dx.doi.org/10.1016/j.jappgeo.2003.08.016.

Jørgensen, F., Lykke-Andersen, H., Sandersen, P.B.E., Auken, E., Nørmark, E. , 2003b. Geophysical investigations of buried quaternary valleys in Denmark: an integrated application of transient electromagnetic soundings, reflection seismic surveys and exploratory drillings. J. Appl. Geophys. 53, 215–228. http://dx.doi.org/10.1016/j.jappgeo.2003.08.017.

Jørgensen, F., Møller, R.R., Sandersen, P.B.E., Nebel, L., 2010. 3-D geological modelling of the Egebjerg area, Denmark, based on hydrogeophysical data. Geol. Surv. DENMARK Greenl. Bull. 27–30.

Kirsch, R., 2009. Groundwater Geophysics : A Tool For Hydrogeology. Springer.

Klise, K.A., Weissmann, G.S., McKenna, S.A., Nichols, E.M., Frechette, J.D., Wawrzyniec, T.F., et al., 2009. Exploring solute transport and streamline connectivity using lidar-based outcrop images and geostatistical representations of heterogeneity. Water Resour. Res. 45. http://dx.doi.org/10.1029/2008WR007500, n/a-n/a.

Koch, J., He, X., Jensen, K.H., Refsgaard, J.C., 2014. Challenges in conditioning a stochastic geological model of a heterogeneous glacial aquifer to a comprehensive soft data set. Hydrol. Earth Syst. Sci. 18, 2907–2923. http://dx.doi.org/10.5194/hess-18-2907-2014.

Linde, N., Renard, P., Mukerji, T., Caers, J., 2015. Geological realism in hydrogeological and geophysical inverse modeling: a review. Adv. Water Resour. 86, 86–101. http://dx.doi.org/10.1016/j.advwatres.2015.09.019.

Marker, P.A., Foged, N., He, X., Christiansen A, V., Refsgaard, J.C., Auken, E., et al., 2015. Performance evaluation of groundwater model hydrostratigraphy from airborne electromagnetic data and lithological borehole logs. Hydrol. Earth Syst. Sci. 19, 3875–3890. http://dx.doi.org/10.5194/hess-19-3875-2015.

Meier, P., Kalscheuer, T., Podgorski, J.E., Kgotlhang, L., Green, A.G., Greenhalgh, S., et al., 2014. Hydrogeophysical investigations in the western and north-central Okavango Delta (Botswana) based on helicopter and ground-based transient electromagnetic data and electrical resistance tomography. Geophysics 79, B201–B211. http://dx.doi.org/10.1190/geo2014-0001.1.

Muffels, C., Wang, X., Matthew Tonkin, A., Neville, C., 2014. User's Guide for mod–PATH3DU a Groundwater Path and Travel-Time Simulator. Bethesda, Maryland.

Neuman, S.P., Yakowitz, S., 1979. A statistical approach to the inverse problem of aquifer hydrology: 1. Theory. Water Resour. Res. 15, 845–860. http://dx.doi.org/10.1029/WR015i004p00845.

Panday, S., Langevin, C.D., Niswonger, R.G., Ibaraki, M., Hughes, J., 2015. An unstructured grid version of MODFLOW for simulating groundwater flow and tightly coupled processes using a control volume finite-difference formulation. In: U.S. Geological Survey Techniques and Methods Reston, Virginia, 6–A45, p. 78.

Pebesma, E.J., 2004. Multivariable geostatistics in S: the gstat package. Comput. Geosci. 30, 683–691.

Purvance, D.T., Andricevic, R., 2000. On the electrical-hydraulic conductivity correlation in aquifers. Water Resour. Res. 36, 2905–2913. http://dx.doi.org/10.1029/2000WR900165.

Rasmussen, P., Sonnenborg, T.O., Goncear, G., Hinsby, K., 2013. Assessing impacts of climate change, sea level rise, and drainage canals on saltwater intrusion to coastal aquifer. Hydrol. Earth Syst. Sci. 17, 421–443. http://dx.doi.org/10.5194/hess-17-421-2013.

Refsgaard, J.C., Christensen, S., Sonnenborg, T.O., Seifert, D., Hojberg, A.L., Troldborg, L., 2012. Review of strategies for handling geological uncertainty in groundwater flow and transport modeling. Adv. Water Resour. 36, 36–50. http://dx.doi.org/10.1016/j.advwatres.2011.04.006.

Ritzi, R.W., 2000. Behavior of indicator variograms and transition probabilities in relation to the variance in lengths of hydrofacies. Water Resour. Res. 36, 3375–3381. http://dx.doi.org/10.1029/2000WR900139.

Rojas, R., Batelaan, O., Feyen, L., Dassargues, A., 2010. Assessment of conceptual model uncertainty for the regional aquifer Pampa del Tamarugal - North Chile. Hydrol. Earth Syst. Sci. 14, 171–192.

Ronayne, M.J., Gorelick, S.M., Caers, J., 2008. Identifying discrete geologic structures that produce anomalous hydraulic response: An inverse modeling approach. Water Resour. Res. 44. http://dx.doi.org/10.1029/2007WR006635, n/a-n/a.

Rubin, Y., Hubbard, S.S., 2005. Hydrogeophysics, 50 editors. Springer Netherlands, Dordrecht http://dx.doi.org/10.1007/1-4020-3102-5.

Søndergaard, V., Thomsen, R., Dyrsø, O., Nyholm, T., Fuglsang, E., Thorling, L., et al., 2004a. Redegørelse for grundvandsressourcerne i Århus-Nord området. Vandforsyning - Delrapport 3, 4–24.

Søndergaard, V., Thomsen, R., Dyrsø, O., Nyholm, T., Fuglsang, E., Thorling, L., et al., 2004b. Redegørelse for grundvandsressourcerne i Århus-Nord området. Vandforsyning - Delrapport 1, 4–38.

Sørensen, K.I., Auken, E., 2004. SkyTEM - a new high-resolution helicopter transient electromagnetic system. Explor. Geophys. 35, 194–202.

Sørensen, K.I., Auken, E., Christensen, N.B., Pellerin, L., 2005. 21. An integrated approach for hydrogeophysical investigations. new technologies and a case history. Near-Surface Geophys. Part II, 585–603. http://dx.doi.org/10.1190/1.9781560801719.ch21.

Sørensen, K., 1996. Pulled array continuous electrical profiling. First Break 14, 85–90.

Seifert, D., Sonnenborg, T.O., Refsgaard, J.C., Hojberg, A.L., Troldborg, L., 2012. Assessment of hydrological model predictive ability given multiple conceptual geological models. Water Resour. Res. 48, W06503. http://dx.doi.org/10.1029/2011wr011149.

Steinmetz, D., Winsemann, J., Brandes, C., Siemon, B., Ullmann, A., Wiederhold, H., et al., 2014. Towards an improved geological interpretation of airborne electromagnetic data: a case study from the Cuxhaven tunnel valley and its Neogene host sediments (northwest Germany). Netherlands J. Geosci. 94, 201–227. http://dx.doi.org/10.1017/njg.2014.39.

Sulzbacher, H., Wiederhold, H., Siemon, B., Grinat, M., Igel, J., Burschil, T., et al., 2012. Numerical modelling of climate change impacts on freshwater lenses on the North Sea Island of Borkum using hydrological and geophysical methods. Hydrol. Earth Syst. Sci. 16, 3621–3643. http://dx.doi.org/10.5194/hess-16-3621-2012.

Tartakovsky, D.M., 2013. Assessment and management of risk in subsurface hydrology: a review and perspective. Adv. Water Resour. 51, 247–260. http://dx.doi.org/10.1016/j.advwatres.2012.04.007.

Viezzoli, A., Christiansen, A.V., Auken, E., Sørensen, K., 2008. Quasi-3D modeling of airborne TEM data by spatially constrained inversion. Geophysics 73, F105–F113. http://dx.doi.org/10.1190/1.2895521.

Vilhelmsen, T.N., 2012. Modeling groundwater flow in geological complex areas using local grid refinement, combined parameterization methods and joint inversion. Aarhus University.